Reaction of the Radical Pair $NO_2^{\bullet}$ and $CO_3^{\bullet-}$ with 2-[6-(4′-Amino)phenoxy-3*H*-xanthen-3-on-9-yl]benzoic Acid (APF)

Adrian Matthew Mak,[†] Matthew Whiteman,[‡] and Ming Wah Wong*[,†]

Department of Chemistry, National University of Singapore, 3 Science Drive 3, Singapore 117543, and Institute of Biomedical and Clinical Science, Peninsula Medical School, Universities of Exeter and Plymouth, St Luke's Campus, Magdalen Road, Exeter, Devon EX1 2LU, England

Received: April 24, 2007; In Final Form: June 20, 2007

The fluorogenic indicator 2-[6-(4′-amino)phenoxy-3*H*-xanthen-3-on-9-yl]benzoic acid (APF) is used widely to detect and measure reactive nitrogen and oxygen species such as peroxynitrite, $ONOO^-$, both in vivo and in vitro. We present in this work the results of a combined computational and experimental study to provide insights into the mechanism of the reaction of APF with the radical products of $ONOO^-$ reaction with CO_2, namely $NO_2^{\bullet}$ and $CO_3^{\bullet-}$. The experimental study on the inhibition of APF oxidation by HCO_3^- suggests that a direct reaction of APF with nitrosoperoxycarbonate, $ONOOCO_2^-$, is unlikely. The mechanism of APF action on $NO_2^{\bullet}$ and $CO_3^{\bullet-}$ was investigated using gas-phase and solvent modeled calculations at the MPW1K/6-311+G(d)//MPW1K/6-31G(d) level of theory. Our computational results suggest that two-electron oxidation of APF takes place in two rapid one-electron oxidation steps, the first being a proton-coupled electron transfer (PCET) between APF and $NO_2^{\bullet}$, followed by addition of $CO_3^{\bullet-}$ and subsequent decomposition of the adduct to yield fluorescein.

1. Introduction

Reactive nitrogen species (RNS) and reactive oxygen species (ROS) play numerous and diverse roles in physiological pathways. RNS and ROS mediate nitrosative and oxidative stress and exhibit both cytotoxic and cytoprotective effects.[1] The RNS peroxynitrite ($ONOO^-$) is a free radical precursor that is formed in cells by diffusion-controlled reaction of nitric oxide ($NO^{\bullet}$) and superoxide ($O_2^{\bullet-}$). The gas-phase reaction enthalpy for the reaction of $NO^{\bullet}$ with $O_2^{\bullet-}$ to form $ONOO^-$ at 298 K was earlier calculated to be -138.3 kJ mol^{-1} at the CCSD(T)/cc-pvQZ//CCSD/cc-pVTZ level.[2] It has been established recently that $ONOO^-$ reacts rapidly with ubiquitous CO_2 ($k = 3 \times 10^4$ M^{-1} s^{-1})[3] to form nitrosoperoxycarbonate anions ($ONOOCO_2^-$), which then undergo O−O bond homolysis to give $NO_2^{\bullet}$ and $CO_3^{\bullet-}$ radicals at a yield of about 30%.[4] These radicals can in turn react with nucleotide bases in DNA and RNA, or amino acid residues in proteins, resulting in significant structural changes and irreversible damage,[5] although such reactions have not been well characterized experimentally. It is widely believed that the action of these RNS and ROS contributes to Alzheimer's disease,[6] Parkinson's disease,[7] atherosclerosis,[8] and cancer.[9]

The detection of RNS and ROS is a difficult task due to two main reasons: their short lifespan and their high reactivity with numerous other molecules. As a consequence, detection, measurement, and monitoring of RNS and ROS levels remain a constant challenge to scientists. Fluorescent probes are highly sensitive and useful in monitoring RNS and ROS. An ideal fluorescent probe should display high fluorescence quantum yield for the species to be detected, and should be both selective and accurate. At present, there are several fluorescent probes commercially available for detecting and measuring $ONOO^-$, for instance, 2′,7′-dicholorofluorescin (DCFH), dihydrofluorescein (HFLUOR), dihydrorhodamine 123 (DHR), rhodamine B hydrazide, 2-[6-(4′-amino)phenoxy-3*H*-xanthen-3-on-9-yl]benzoic acid (APF),[10] and the more recently developed HKGreen-1.[11] In particular, Setsukinai et al. have shown that APF exhibits excellent selectivity for $ONOO^-$ over other radicals and radical precursors such as $NO^{\bullet}$, $O_2^{\bullet-}$, hydrogen peroxide (H_2O_2), and alkyl peroxide radicals ($ROO^{\bullet}$) when compared with DCFH.[12] APF molecule undergoes *O*-dearylation in the presence of RNS generated by $ONOO^-$ derivatives to yield fluorescein, with excitation and emission wavelengths of 490 and 520 nm, respectively (Scheme 1). Although these probes are known to be oxidized to their fluorescent forms in the presence of $ONOO^-$, information on the exact identities of the species that react with these probes is lacking.

SCHEME 1: Action of RNS on APF, Adapted from Ref 12

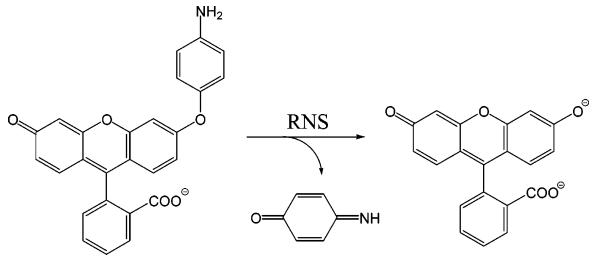

Experiments carried out by various research groups have shed some light on the mechanism of fluorescent probe oxidation by $ONOO^-$ and its derivatives. The exclusion of a direct reaction of $ONOO^-$ with a fluorescent probe was established by Jourd'heuil et al.[13] The authors demonstrated that the oxidation of DHR by $ONOO^-$ occurs via free radical intermediates $NO_2^{\bullet}$ and $OH^{\bullet}$ formed from the spontaneous decomposition of ONOOH. Kinetic studies by Koppenol et al. reveal that reaction

* Corresponding author. E-mail: chmwmw@nus.edu.sg.
[†] National University of Singapore.
[‡] Universities of Exeter and Plymouth.

10.1021/jp073142p CCC: $37.00
Published on Web 08/02/2007

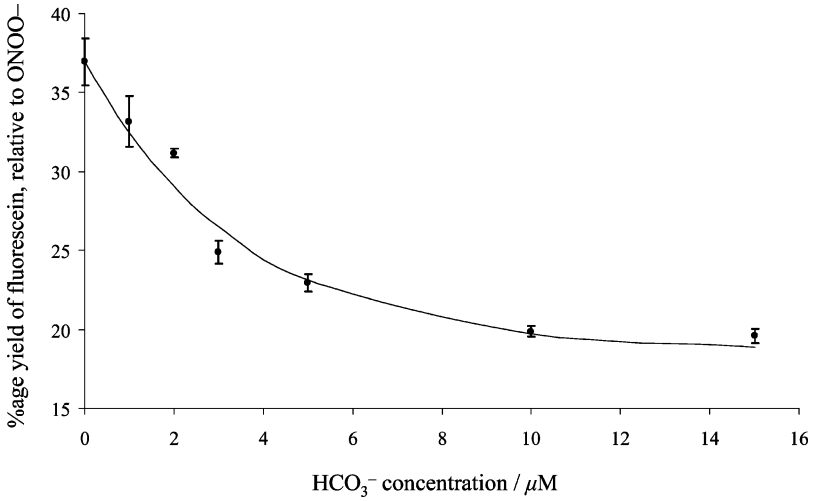

Figure 1. Plot of percentage yield of fluorescein, relative to $ONOO^-$, vs the concentration of HCO_3^- in the reaction mixture. Other experimental conditions: 10 μM APF, 1.0 μM $ONOO^-$, 0.1 M phosphate buffer at pH 7.4. Total volume of the mixture is 1 mL.

SCHEME 2: Pathway I of APF Oxidation

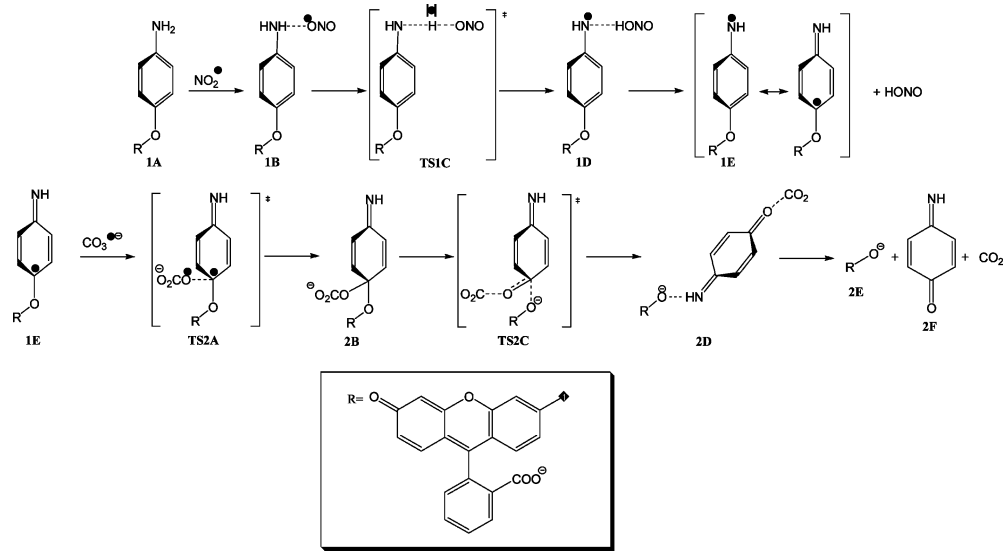

of DCFH with $ONOO^-$ is essentially zero order with respect to the indicator, eliminating the possibility of a direct reaction between $ONOO^-$ and the probe molecule.[14] They proposed that the reactive species that oxidized DCFH is the radical pair $NO_2^{\bullet}$ and $CO_3^{\bullet-}$.

Despite the fact that APF is used by many research groups to detect and measure $ONOO^-$ in various experiments, both in vivo and in vitro, the reasons for which APF exhibits selectivity for $ONOO^-$ over other RNS and ROS are still unclear. In this paper, a computational study of the reaction of APF with $NO_2^{\bullet}$ and $CO_3^{\bullet-}$ is presented to shed some light into its reaction mechanism and the factors that influence the selectivity of the probe. An experimental examination of the influence of HCO_3^- concentration on the $ONOO^-$ mediated two-electron oxidation of APF was also carried out to better understand the chemistry pertinent to this intriguing reaction.

2. Methods

2.1. Computational Methods. A hybrid DFT method, the modified Perdew−Wang one-parameter method for kinetics (MPW1K), was employed in this study. Hybrid DFT methods have been shown to be successful in obtaining accurate molecular geometries, vibrational frequencies and bond energies.[15] The MPW1K functional was parametrized to yield improved performance for kinetics calculations and bond energies as compared to other hybrid DFT functionals such as B3LYP, BH&HLYP, and mPWPW91.[16] In particular, the MPW1K functional yields improved accuracy in transition state geometries and barrier heights compared to the abovementioned functionals,[17] making the MPW1K method an adequate choice for investigating the system in question.

Full geometry optimizations of all local minima and saddle points were carried out at the MPW1K/6-31G(d) level of theory. Frequency calculations for all species were carried out to verify if they were indeed local minima with all real frequencies or first-order saddle points (i.e., transition states) with one imaginary frequency. Closed- and open-shell species were treated using the RHF and UHF formalisms, respectively. Additional energy calculations were carried out at the MPW1K/6-311+G-(d,p) level, based on the MPW1K/6-31G(d) optimized geometry, to obtain a more accurate estimate of the energetics of the reaction studied. The energies of open-shell species were also spin-corrected using the method developed by Yamaguchi et al.[18]

SCHEME 3: Pathway II of APF Oxidation

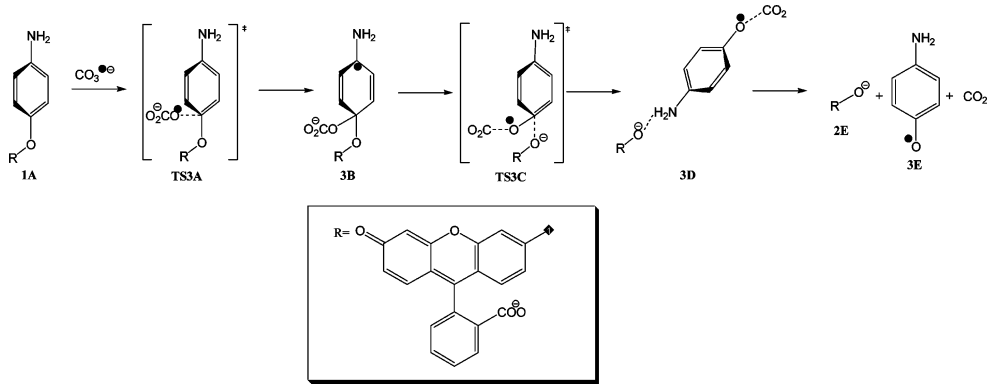

The polarizable continuum model of Tomasi et al.[19] (PCM) was initially used to investigate the effect of a solvent reaction field on the energetics of the reaction studied. However, convergence problems were encountered in the optimization of structures. Hence, geometry optimizations and frequency calculations were carried out for selected local minima and transition states using the more robust Onsager reaction field (SCRF = dipole) method[20] at the MPW1K/6-31G(d) level. A dielectric constant (ϵ) of 40.0 is used to model a polar medium. For a molecular ion with a total charge Q, a Born charge term,[21] $-1/2(1 - 1/\epsilon)Q^2/a_0$ (where a_0 is the cavity radius), was added to the expression of solvation energy to account for the ion−dipole interaction. It is important to note that the SCRF is not a suitable method to model aqueous solvation where specific solvent−solute interaction is expected to be important. Therefore, the scope of present solvation study is limited to an aprotic polar solvent such as acetonitrile. Higher-level relative energies were obtained using this solvation model at the MPW1K/6-311+G(d,p) level, together with spin-correction for open-shell species. All calculations were performed using the GAUSSIAN 03[22] program suite.

2.2. Experimental Methods. APF {2-[6-(4′-amino)phenoxy-3*H*-xanthen-3-on-9-yl]benzoic acid} was purchased from Alexis Corporation (Lausen, Switzerland). All other chemicals were obtained from Sigma Ltd. (St Louis, MO) and freshly prepared on the day of the experiment. Distilled water passed through a Millipore water purification system was used for all purposes.

Sodium phosphate buffer (0.1 M) at pH 7.4 and sodium hydrogen carbonate solution (0.25 M) were added along with 2 μL of stock APF solution into 1 mL sample tubes and protected from light. This mixture is allowed to stand for about 15 min to allow equilibration of hydrogen carbonate, carbon dioxide, and carbonate in solution before other reagents were added. Hydrogen peroxide-free peroxynitrite was prepared using the method described by Beckman et al.[23] Removal of residual H_2O_2 was confirmed using a commercial kit (Amplex Red; Molecular Probes).[24] Concentrations of $ONOO^-$ were redetermined before each experiment using UV−visible spectroscopy, with $ONOO^-$ having a molar extinction coefficient, $\epsilon = 1670$ cm^{-1}, at 302 nm. $ONOO^-$ concentrations of 250−300 mM were usually obtained. This concentrated peroxynitrite (about 2−5 μL) was then added to the reaction mixture in the sample tube. The sample tubes were then vortexed and left to stand for 5 min before the fluorescence intensity was measured. The pH of the well-buffered reaction mixture upon adding of a small amount of concentrated peroxynitrite is not expected to significantly change, as already reported in previous work.[25] Final concentrations of the components in the reaction mixture after mixing were: 10 μM APF, 1.0 μM $ONOO^-$, 0.1 M phosphate buffer, and varying concentrations of HCO_3^-, from 0 to 25 mM. The fluorescence intensity that resulted from peroxynitrite-mediated oxidation of APF was monitored with $\lambda_{excitation} = 490$ nm and $\lambda_{emission} = 520$ nm at room temperature, using a Gemini EM fluorescence microplate reader from Molecular Devices.

3. Results and Discussion

3.1. Influence of HCO_3^- Concentration on $ONOO^-$ Mediated Oxidation of APF. In an attempt to obtain some insight as to whether HCO_3^- substantially influences the $ONOO^-$ mediated oxidation of APF, we studied the percentage yield of fluorescein as a function of $[HCO_3^-]$. It was found that, with increasing concentrations of HCO_3^- in solution, oxidation of APF was inhibited, although not completely (Figure 1). This finding is consistent with the results obtained by Koppenol et al. for the fluorogenic indicators DCFH and DHR.[14] Increasing $[HCO_3^-]$ shifts the equilibrium of the reaction $HCO_3^- = CO_2 + OH^-$ farther to the right, and the increased CO_2 concentration leads to the formation of larger amounts of $ONOOCO_2^-$ from the reaction $ONOO^- + CO_2 = ONOOCO_2^-$. The observation that increasing $[HCO_3^-]$ progressively lowers the yield of fluorescent products instead of increasing it appears to exclude the pathway where APF reacts directly with $ONOOCO_2^-$. A similar conclusion with that by Koppenol et al.[14] is thus reached, that the direct reaction between APF and $ONOOCO_2^-$ is not likely.

The O—O bond dissociation energy (BDE) of $ONOOCO_2^-$ was previously estimated at the CBS-QB3 level to be 31.4 kJ mol^{-1}.[26] This magnitude of O—O BDE in $ONOOCO_2^-$ is unexpectedly low compared to O—O BDEs in other compounds such as hydrogen peroxide HO−OH (213.4 kJ mol^{-1}), dimethyl peroxide CH_3O-OCH_3 (158.6 kJ mol^{-1}), and pernitric acid $HO-ONO_2$ (163.2 kJ mol^{-1}).[27] The relative ease of decomposition of $ONOOCO_2^-$ supports the explanation proposed by Koppenol et al. for the DCFH and DHR case, that these fluorogenic indicators react with that the decomposition products of $ONOOCO_2^-$, namely the radical pair $NO_2^\bullet$ and $CO_3^{\bullet -}$.[14] This explanation can be extended for the fluorogenic indicator APF.

3.2. Gas-Phase Calculations. The final product, fluorescein, can exist in a number of structural (quinoid, zwitterionic, and lactoid) and prototropic (neutral, monoanionic, and dianionic) forms. It exists purely as the dianionic form at pH 9.1 and the monoanionic form at pH 5.4. At pH 7.4, fluorescein exists as a mixture of both forms.[28] Quantum mechanical studies on the charge-transfer transition for both forms show that the transition for the dianion has markedly higher oscillator strength than that for the monoanion.[29] Thus, the monoanionic carboxylate form of APF, which yields dianionic fluorescein after oxidation, was employed in this study.

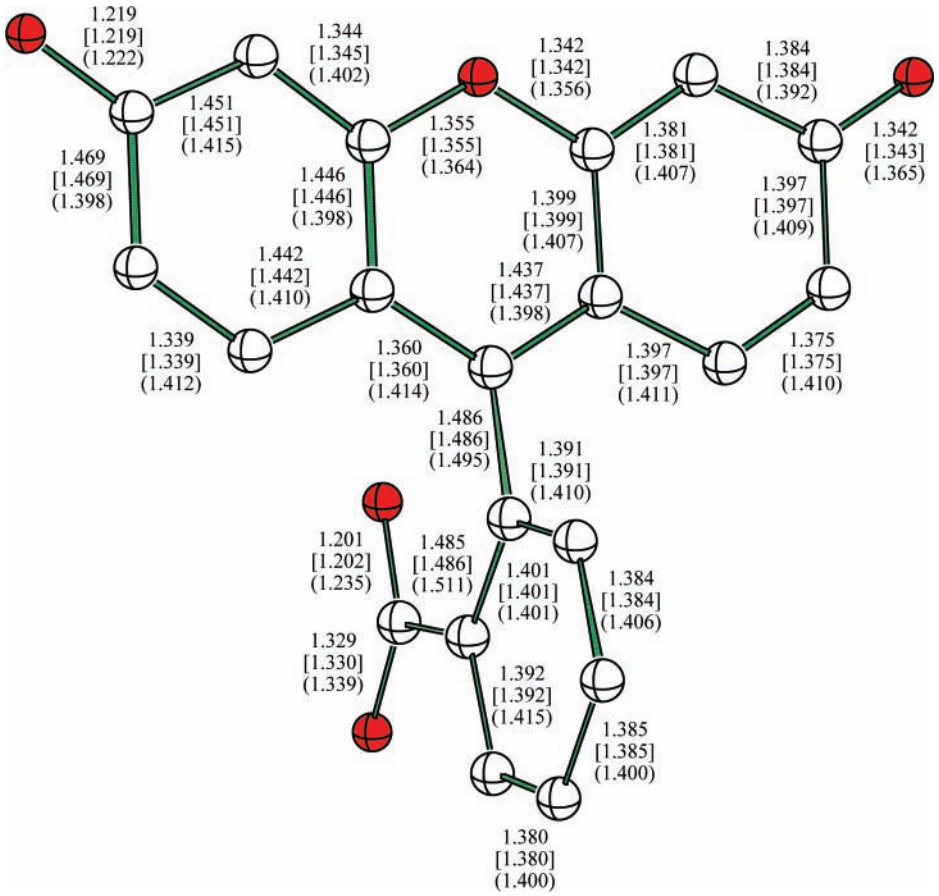

Figure 2. Calculated structural parameters of dianionic fluorescein, **2E**, at the MPW1K/6-31G(d) level in the gas phase. Calculated structural parameters for neutral fluorescein at the MPW1K/6-31G(d) level are given in square brackets. X-ray structural parameters (from ref 29) are given in parentheses. Nonessential hydrogens are omitted for clarity. Distances are in Å. Oxygen atoms are in dark color.

On the basis of the two-electron oxidation products of APF reaction with RNS, namely fluorescein and *p*-benzoquinone imine, and the reactive species $NO_2^{\bullet}$ and $CO_3^{\bullet-}$ involved as reactants, the reaction of APF can be interpreted as sequences of reactions illustrated in Schemes 2 and 3. The reaction can occur via two plausible pathways. The first, pathway I (Scheme 2), involves two rapid one-electron oxidations. The first one-electron oxidation step involves a proton-coupled electron transfer (PCET) from the amino group in APF (**1A**) by $NO_2^{\bullet}$. The second step involves O^- addition by $CO_3^{\bullet-}$ to form the resonance-stabilized anilinyl fluorescein radical **1E**, followed by decomposition of the adduct **2B** to yield fluorescein, **2E**, *p*-benzoquinone imine, **2F**, and CO_2. The second pathway, pathway II (Scheme 3), involves a direct addition of $CO_3^{\bullet-}$ to **1A** to give a radical adduct **3B**. Decomposition of the adduct yields **2E**, *p*-aminophenoxyl radical, **3E**, and CO_2.

The calculated structural parameters of neutral fluorescein (Figure 2), are in good accord with known experimental values,[30] with maximum relative errors for bond lengths at 5%. Calculated structural parameters of dianionic fluorescein **2E** are essentially identical to those of the neutral form. A comparison of 11 known vibrational modes of fluorescein[28] with the calculated MPW1K/6-31G(d) frequencies yielded errors between 4 and 18%. However, upon applying a frequency scaling factor of 0.905, the relative errors were reduced to 1.1−5.7%. The relatively good agreement of calculated geometries and frequencies with experimental values provided the confidence that the choice of the MPW1K/6-31G(d) method is adequate for the study of the reaction in question. With the lack of reliable zero-point energy data for fluorescein, the scaling factor for fundamentals was applied to calculated the zero-point vibrational energies.

Gas-phase transition energy ($\lambda_{excitation}$) for dianionic fluorescein was calculated using ZINDO/S[31] and TD−DFT[32] methods. The predicted $\lambda_{excitation}$ using the ZINDO/S method is 475 nm, in close agreement with the experimental value of 490 nm.[33] TD-B3LYP/6-311+G(d,p)//B3LYP/6-31G(d) and TD-MPW1K/6-311+G(d,p)//MPW1K/6-31G(d) predict $\lambda_{excitation}$ values of 430 and 392 nm, respectively. It is important to note that time-dependent density-functional theory yields unsatisfactory results for excitation energies of long-range charge-transfer states.[34]

Schematic energy profiles of the APF oxidation reactions in the gas phase, calculated at MPW1K/6-311+G(d,p)//MPW1K/6-31G(d) + ZPE level, are presented in Figures 3−5. Gas-phase MPW1K/6-31G(d) optimized structures of selected local minima (**1A**, **1B**, **1D**, **1E**, **2B**, **2D**, **3B**, **3D**, and **3E**) and all transition

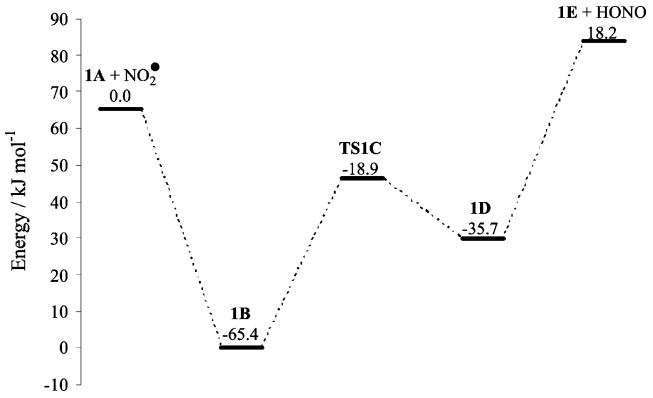

Figure 3. Schematic gas-phase reaction energy profile for step 1 of pathway I, calculated at the MPW1K/6-311+G(d,p)//MPW1K/6-31G(d)+ZPE level with spin correction.

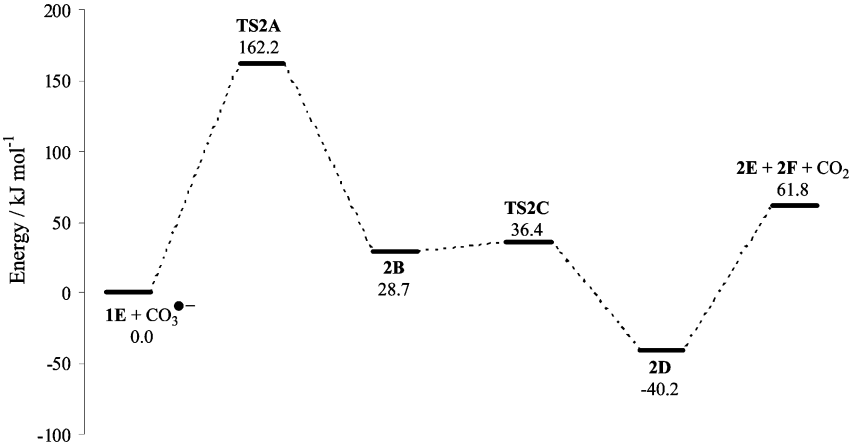

Figure 4. Schematic gas-phase reaction energy profile for step 2 of pathway I, calculated at the MPW1K/6-311+G(d,p)//MPW1K/6-31G(d)+ZPE level with spin correction.

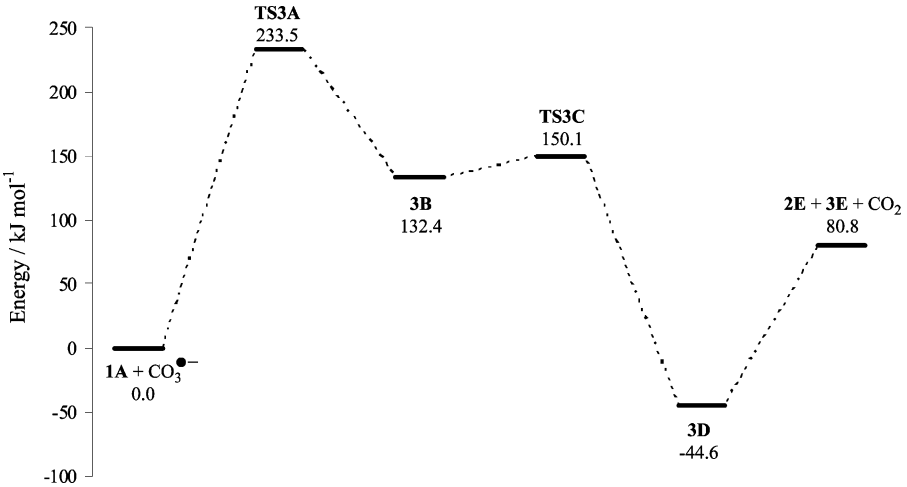

Figure 5. Schematic gas-phase reaction energy profile for pathway II, calculated at the MPW1K/6-311+G(d,p)//MPW1K/6-31G(d)+ZPE level with spin correction

.

states (**TS1C**, **TS2A**, **TS2C**, **TS3A**, and **TS3C**) are presented in Figures 6 −8. The atom numbering scheme used for **1A**, **1E**, **TS2C**, and **TS3C** is given in Figure 9.

In pathway I, $NO_2^\bullet$ first interacts with **1A** to form a hydrogen-bonded reactant complex **1B**, with a relatively large binding energy of 65.4 kJ mol^{-1}. The hydrogen transfer reaction involves the transfer of the amino hydrogen of **1B** to $NO_2^\bullet$. It occurs via **TS1C**, with an activation barrier of 46.5 kJ mol^{-1}. The N···H and O···H bond distances in **TS1C** are 1.143 and 1.367 Å, respectively. The N···H···O moiety is close to linearity (Figure 8). Because of the larger interaction of the pretransition state complex **1B**, the hydrogen transfer reaction has a negative barrier with respect to **1A** + $NO_2^\bullet$. The hydrogen-bonded product complex **1D** is slightly less stable than the reactant complex **1B** by 29.7 kJ mol^{-1}.

It is important to note that carbonate radical anion ($CO_3^{\bullet-}$) is a strong one-electron oxidant that oxidizes appropriate electron donors via electron-transfer mechanisms.[35] The redox potential of $CO_3^{\bullet-}$ (eq 1) is well established[36] and is strongly positive, 1.6 V (pH 12.5) to 1.78 V (pH 7.0). In fact, this value is greater than the redox potential of $NO_2^\bullet$ (eq 2).[37]

$$CO_3^{\bullet-} + e^- + H^+ \rightarrow HCO_3^- \; E^\circ = 1.78 \text{ V vs NHE} \quad (1)$$

$$NO_2^\bullet + e^- \rightarrow NO_2^- \; E^\circ \approx 1.04 \text{ V vs NHE} \quad (2)$$

Thus, the first one-electron oxidation step of pathway I may involve $CO_3^{\bullet-}$ (eq 3).

$$\mathbf{1A} + CO_3^{\bullet-} \rightarrow \mathbf{1E} + HCO_3^- \quad (3)$$

The proton coupled electron transfer (PCET) from the amino group in APF (**1A**) by $CO_3^{\bullet-}$ will also lead to **1E** together with HCO_3^-, a fairly stable bicarbonate anion. The calculated reaction energy of this one-electron oxidation reaction is exothermic by 45.0 kJ mol^{-1}. However, this electron-transfer reaction is expected to be unfavorable kinetically as the transition state involves two anions approach each other. Indeed, this proton-coupled electron-transfer reaction is calculated to have a large barrier of 106.9 kJ mol^{-1}. The dianion transition state is significantly higher in energy (by 125.8 kJ mol^{-1}) compared to the transition state involving $NO_2^\bullet$ (**TS1C**). This result suggests that the alternate one-electron oxidation via carbonate radical anion is less viable.

The $CO_3^{\bullet-}$ radical can add to **1E** in three plausible positions: C(23), C(25), and C(27) (see Figure 9). The only position involving $CO_3^{\bullet-}$ radical addition to yield the final products is at C(23) and, hence, is the only one considered here. Addition of the $CO_3^{\bullet-}$ radical to **1E** to form adduct **2B** is endothermic by 28.7 kJ mol^{-1} and proceeds via a transition state **TS2A** with strong biradical character. The forming C···O bond length in

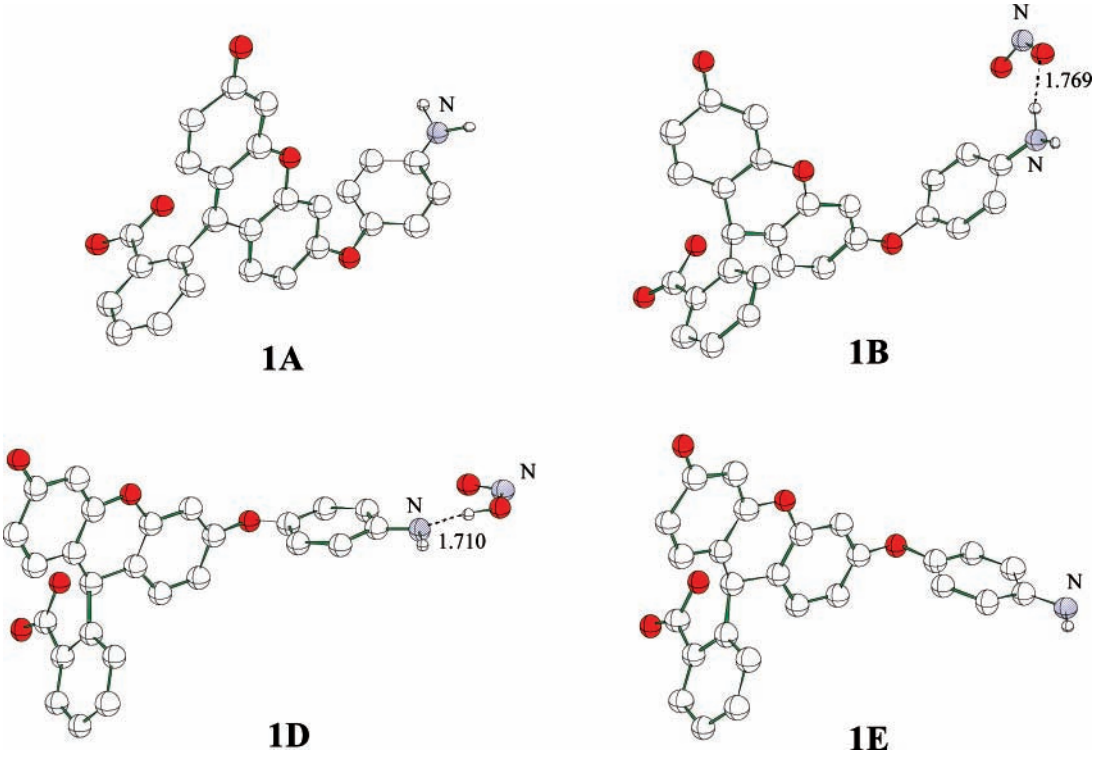

Figure 6. MPW1K/6-31G(d) optimized geometries of **1A**, **1B**, **1D**, and **1E**. Distances shown are in Å. Nonessential hydrogens are omitted for clarity. Oxygen atoms are in dark color.

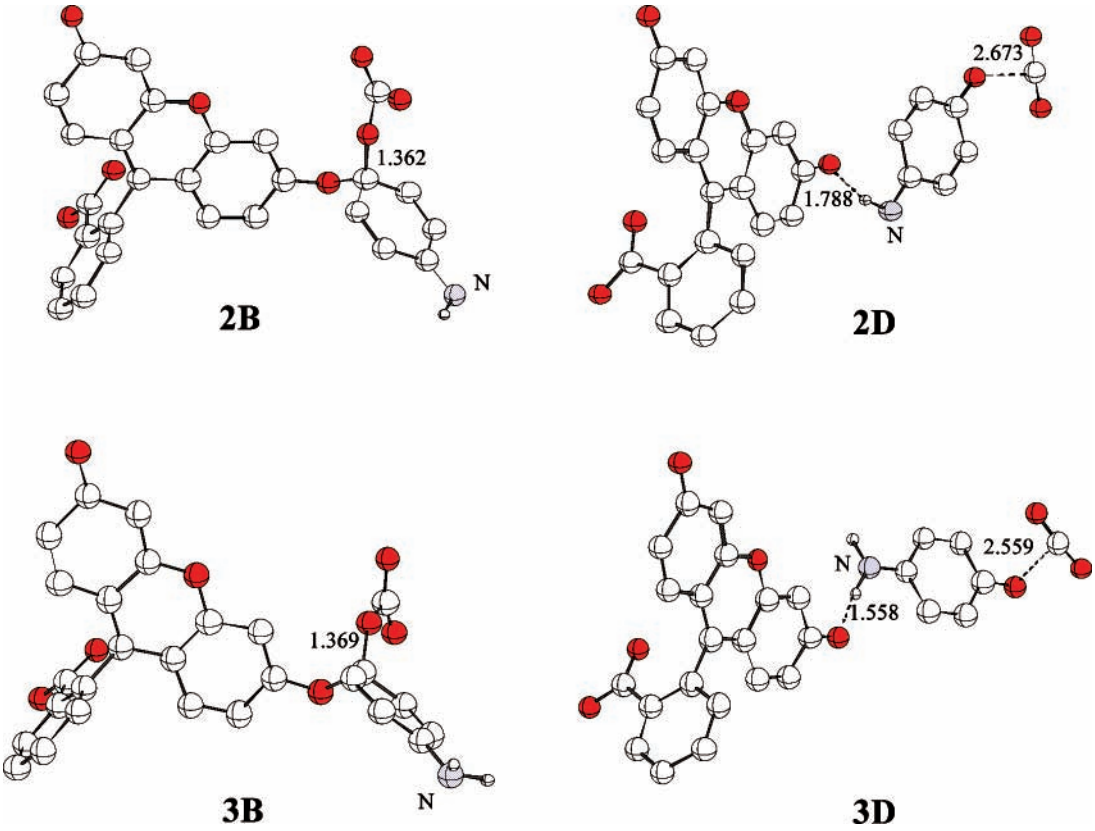

Figure 7. MPW1K/6-31G(d) optimized geometries of **2B**, **2D**, **3B**, and **3D**. Distances shown are in Å. Nonessential hydrogens are omitted for clarity. Oxygen atoms are in dark color.

TS2A is 2.035 Å. The expectation value of the spin-squared operator $\langle S^2 \rangle$ of **TS2A** is 0.742, indicating that there is a significant degree of spin contamination from the higher-energy spin states. The activation barrier for $CO_3^{\bullet-}$ addition via **TS2A** before spin correction is 193.0 kJ mol^{-1}. After the addition of the spin correction term, this barrier is reduced significantly to 162.2 kJ mol^{-1}.

Decomposition of **2B** to form **2E**, **2F**, and CO_2 is endothermic by 33.1 kJ mol^{-1} and takes place via **TS2C**. Two C—O bonds break simultaneously between C(23) and O(22) and between

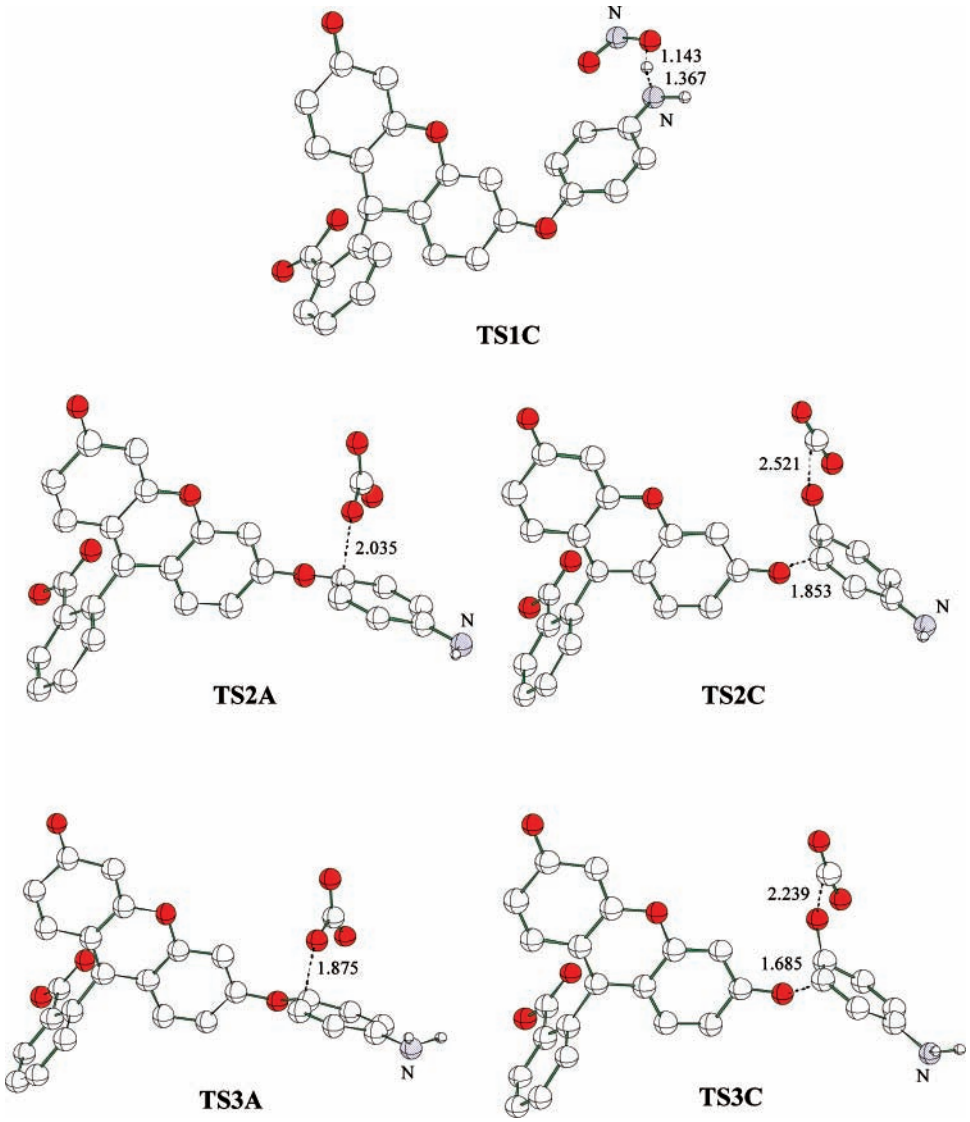

Figure 8. MPW1K/6-31G(d) optimized geometries of transition structures **TS1C**, **TS2A**, **TS2C**, **TS3A**, and **TS3C**. Distances shown are in Å. Nonessential hydrogens are omitted for clarity. Oxygen atoms are in dark color.

C(31) and O(30) in **TS2C** (see Figure 8). C(23)—O(22) and C(31)—O(30) distances are 1.853 and 2.521 Å, respectively, in **TS2C**. Remarkably, this fragmentation process is inhibited by a small barrier of just 7.7 kJ mol^{-1}. As expected, the final products form a stable complex **2D** (**2E**$\cdots$**2F**$\cdots$$CO_2$) with a fairly large binding energy of 102.0 kJ mol^{-1}.

The radical addition process via pathway II is similar to the second step of pathway I. The $CO_3^{\bullet-}$ radical is expected to undergo radical addition with the initial reactant **1A** instead of the intermediate formed after hydrogen transfer. As with pathway I, the site considered for $CO_3^{\bullet-}$ addition is at C(23). The direct addition of $CO_3^{\bullet-}$ radical anion to **1A** to form **3B** is highly endothermic by 132.4 kJ mol^{-1}. The activation barrier for this process is notably high at 233.5 kJ mol^{-1} via **TS3A**. The transition state of this reaction, **TS3C**, has similar structural characteristics as **TS2C** of pathway I. The C(23)—O(22) and C(31)—O(30) distances in **TS3C** are comparatively shorter, at 1.685 and 2.239 Å, respectively. The products **2E**, **3E**, and CO_2 form a complex with substantial binding energy of 125.4 kJ mol^{-1}. Overall, addition of $CO_3^{\bullet-}$ to **1A** to form **3B** is the rate-determining step of pathway II.

On the basis of the calculated gas-phase potential energy surface, oxidation of APF to form fluorescein can take place via two pathways. Pathway I involves initial proton-coupled electron transfer (PCET) from APF to $NO_2^{\bullet}$, followed by $O^{\bullet-}$ addition of $CO_3^{\bullet-}$ to the radical **1E**, which, with a barrier of 162.2 kJ mol^{-1}, is the rate-limiting step. Pathway II is independent of $NO_2^{\bullet}$ but is not likely to proceed due to a prohibitively high barrier of 233.5 kJ mol^{-1} for the rate-determining step.

3.3. Solvent Effects. To investigate the influence of a solvent reaction field on the reaction mechanism, species **1A**, **1B**, **1E**, **2B**, **3B**, **TS1C**, **TS2A**, **TS2C**, **TS3A**, and **TS3C** were re-optimized at the MPW1K/6-31G(d) level incorporated with the Onsager reaction field model with a dielectric medium of $\epsilon = 40.0$ (representing an aprotic polar solvent). The MPW1K/6-311+G(d,p)//MPW1K/6-31G(d) activation barriers corresponding to **1B** $\rightarrow$ **TS1C**, **1E** + $CO_3^{\bullet-}$ $\rightarrow$ **TS2A**, **2B** $\rightarrow$ **TS2C**, **1A** + $CO_3^{\bullet-}$ $\rightarrow$ **TS3A**, and **3B** $\rightarrow$ **TS3C** in the solvent medium are presented in Table 1, with the gas-phase MPW1K/6-311+G(d,p)//MPW1K/6-31G(d) barriers shown alongside for comparison.

There are small structural changes of various equilibrium structures and transition states on going from the gas phase to a polar dielectric medium. For pathway I, activation barriers **1B** $\rightarrow$ **TS1C** and **1E** + $CO_3^{\bullet-}$ $\rightarrow$ **TS2A** decreased by 19.2 and 101.3 kJ mol^{-1}, respectively, in a polar medium. The vast decrease in barrier height for **1E** + $CO_3^{\bullet-}$ $\rightarrow$ **TS2A** is due

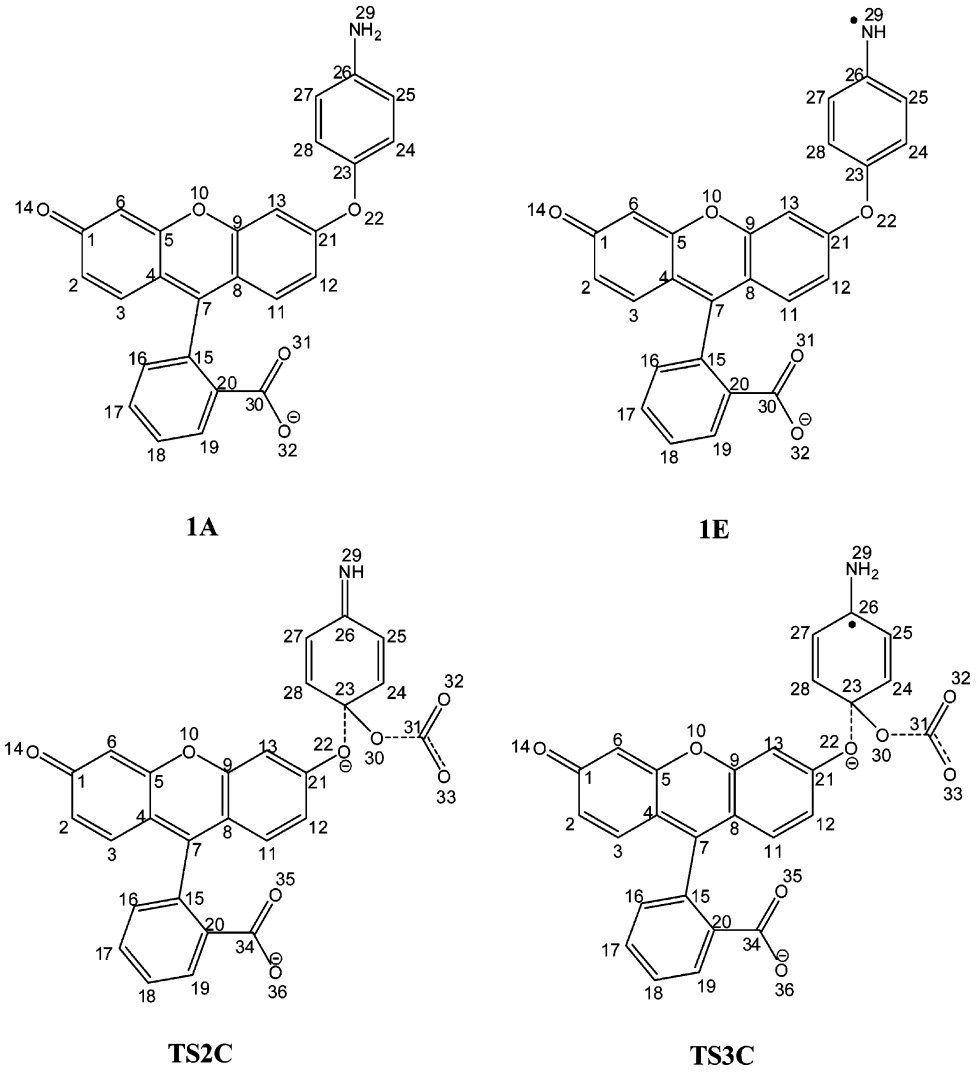

Figure 9. Atom numbering scheme for **1A**, **1E**, **TS2C**, and **TS3C** used in this study.

TABLE 1: Calculated Activation Barriers (kJ mol^{-1}) of the Two Reaction Pathways in the Gas Phase and in a Polar Medium[a]

reaction	gas phase ($\epsilon = 1$)	polar medium ($\epsilon = 40$)[b]
pathway I		
1B → **TS1C**	46.4	27.2
1E + $CO_3^{\bullet-}$ → **TS2A**	162.2	60.9
2B → **TS2C**	7.7	44.1
pathway II		
1A + $CO_3^{\bullet-}$ → **TS3A**	233.5	218.2
3B → **TS3C**	17.7	19.5

[a] MPW1K/6-311+G(d,p)//MPW1K/6-31G(d) + ZPE level. [b] SCRF = dipole calculations.

mainly to the additional contribution of an ion−dipole (Born charge) term in the dianion transition state **TS2A**. The barrier for **2B** → **TS2C** in the polar dielectric medium, on the other hand, increased by 36.4 kJ mol^{-1}. The rate-limiting step is still the addition of $CO_3^{\bullet-}$ radical to **1E**. However, APF oxidation via pathway I is generally more favorable in solvent than in the gas phase, with barriers ranging from 27.2 to 60.9 kJ mol^{-1}.

For pathway II, the activation barrier **1A** + $CO_3^{\bullet-}$ → **TS3A** is lowered by 15.3 kJ mol^{-1}, and the barrier **3B** → **TS3C** is slightly increased by 1.8 kJ mol^{-1}. Comparing with pathway I, pathway II is less likely to proceed because of the prohibitively high barrier of $CO_3^{\bullet-}$ radical addition to **1A**.

4. Concluding Remarks

The reaction of APF with the radicals generated by the reaction of $ONOO^-$ and CO_2, namely $NO_2^{\bullet}$ and $CO_3^{\bullet-}$, was explored. Experimentally, HCO_3^- was found to inhibit the two-electron oxidation of APF, suggesting that the direct reaction of APF with $ONOOCO_2^-$ is unlikely. Two possible pathways of APF oxidation were explored using DFT calculations. Pathway I involves initial proton-coupled electron transfer from APF to NO_2 to obtain a resonance-stabilized anilinyl fluorescein radical. $CO_3^{\bullet-}$ addition to this radical follows and, subsequently, decomposition of the adduct yields fluorescein, *p*-benzoquinone imine, and CO_2. Pathway II involves the direct addition of $CO_3^{\bullet-}$ to APF and the subsequent decomposition of the APF-$CO_3^{\bullet-}$ adduct to form fluorescein, *p*-aminophenoxyl radical, and CO_2. Addition of $CO_3^{\bullet-}$ is the rate-determining step in both pathways, and the activation barrier for this step in pathway II is prohibitively high even in an aprotic polar solvent. Hence, the two-electron oxidation of APF is likely to involve two one-electron oxidations by both $NO_2^{\bullet}$ and $CO_3^{\bullet-}$ radicals and proceeds via pathway I.

Acknowledgment. We are grateful to the Institute of High Performance Computing (IHPC) of the Agency for Science, Technology and Research (A*STAR), Singapore, for the use of their computing resources. This work is supported by the National University of Singapore.

Supporting Information Available: Cartesian coordinates and absolute energies of all calculated compounds. This material is available free of charge via the Internet at http://pubs.acs.org.

References and Notes

(1) Wink, D. A.; Mitchell, J. B. *Free Radical Biol. Med.* **1998**, *25*, 434.

(2) Mak, A. M.; Wong, M. W. *Chem. Phys. Lett.* **2005**, *403*, 192.

(3) Lymar, S. V.; Hurst, J. K. *J. Am. Chem. Soc.* **1995**, *117*, 8867.

(4) (a) Squadrito, G. L.; Pryor, W. A. *Free Radical Biol. Med.* **1998**, *25*, 392. (b) Bonini, M. G.; Radi, R.; Ferrer-Sueta, G.; Da, C.; Ferreira, A. M.; Augusto, O. *J. Biol. Chem.* **1999**, *274*, 10802. (c) Radi, R.; Peluffo, G.; Alvarez, M. N.; Naviliat, M.; Cayota, A. *Free Radical Biol. Med.* **2001**, *30*, 463. (d) Goldstein, S.; Czapski, G.; Lind, J.; Merényi, G. *Chem. Res. Toxicol.* **2001**, *14*, 1273.

(5) Augusto, O.; Bonini, M.; Amanso, A. M.; Linares, E.; Santos, C. C. X.; De Menezes, S. L. *Free Radical Biol. Med.* **2002**, *32*, 841.

(6) Butterfield, D. A. *Free Radical Res.* **2002**, *36*, 1307.

(7) Riobó, N. A.; Schöpfer, F. J.; Boveris, A. D.; Cadenas, E.; Poderoso, J. J. *Free Radical Biol. Med.* **2002**, *32*, 115.

(8) Halliwell, B. *Cardiovasc. Res.* **2000**, *47*, 410.

(9) (a) Hagen, T. M.; Huang, S.; Curnutte, J.; Fowler, P.; Martinez, V.; Wehr, C. M.; Ames, B. N.; Chisari, F. V. *Proc. Natl. Acad. Sci. U.S.A.* **1994**, *91*, 12808. (b) Wink, D. A.; Mitchell, J. B. *Free Radical Biol. Med.* **2003**, *34*, 951.

(10) (a) Halliwell, B.; Whiteman, M. *Br. J. Pharmacol.* **2004**, *142*, 231. (b) Gomes, A.; Fernandes, E.; Lima, J. L. F. C. *J. Fluoresc.* **2006**, *16*, 119.

(11) Yang, D.; Wang, H.-L.; Sun, Z-.N.; Chung, N.-W.; Shen, J.-G. *J. Am. Chem. Soc.* **2006**, *128*, 6004.

(12) Setsukinai, K-I.; Urano, Y.; Kakinuma, K.; Majima, H. J.; Nagano, T. *J. Biol. Chem.* **2003**, *278*, 3170.

(13) Jourd'heuil, D.; Jourd'heuil, F. L.; Kutchukian, P. S.; Musah, R. A.; Wink, D. A.; Grisham, M. B. *J. Biol. Chem.* **2001**, *276*, 28799.

(14) Glebska, J.; Koppenol, W. H. *Free Radical Biol. Med.* **2003**, *35*, 676.

(15) Raghavachari, K. *Theor. Chem. Acc.* **2000**, *103*, 361.

(16) Lynch, B. J.; Fast, P. L.; Harris, M.; Truhlar, D. G. *J. Phys. Chem. A* **2000**, *104*, 4811.

(17) Lynch, B. J.; Truhlar, D. G. *J. Phys. Chem. A* **2001**, *105*, 2936.

(18) (a) Yamanaka, S.; Kawakami, T.; Nagao, H.; Yamaguchi, K. *Chem. Phys. Lett.* **1994**, *231*, 25. (b) Yamaguchi, K.; Jensen, F.; Dorigo, A.; Houk, K. N. *Chem. Phys. Lett.* **1988**, *149*, 537.

(19) (a) Cancès, E.; Mennucci, B.; Tomasi, J. *J. Chem. Phys.* **1997**, *107*, 3032. (b) Cossi, M.; Barone, V.; Mennucci, B.; Tomasi, J. *Chem. Phys. Lett.* **1998**, *286*, 253. (c) Mennucci, B.; Tomasi, J. *J. Chem. Phys.* **1997**, *106*, 5151.

(20) (a) Wong, M. W.; Frisch, M. J.; Wiberg, K. B. *J. Am. Chem. Soc.* **1991**, *113*, 4776. (b) Wong, M. W.; Wiberg, K. B.; Frisch, M. J. *J. Chem. Phys.* **1991**, *95*, 8991. (c) Wong, M. W. Wiberg, K. B.; Frisch, M. J. *J. Am. Chem. Soc.* **1992**, *114*, 1645.

(21) Born, M. *Z. Phys.* **1920**, *1*, 45.

(22) Frisch, M. J.; Trucks, G. W.; Schlegel, H. B.; Scuseria, G. E.; Robb, M. A.; Cheeseman, J. R.; Montgomery, J. A., Jr.; Vreven, T.; Kudin, K. N.; Burant, J. C.; Millam, J. M.; Iyengar, S. S.; Tomasi, J.; Barone, V.; Mennucci, B.; Cossi, M.; Scalmani, G.; Rega, N.; Petersson, G. A.; Nakatsuji, H.; Hada, M.; Ehara, M.; Toyota, K.; Fukuda, R.; Hasegawa, J.; Ishida, M.; Nakajima, T.; Honda, Y.; Kitao, O.; Nakai, H.; Klene, M.; Li, X.; Knox, J. E.; Hratchian, H. P.; Cross, J. B.; Bakken, V.; Adamo, C.; Jaramillo, J.; Gomperts, R.; Stratmann, R. E.; Yazyev, O.; Austin, A. J.; Cammi, R.; Pomelli, C.; Ochterski, J. W.; Ayala, P. Y.; Morokuma, K.; Voth, G. A.; Salvador, P.; Dannenberg, J. J.; Zakrzewski, V. G.; Dapprich, S.; Daniels, A. D.; Strain, M. C.; Farkas, O.; Malick, D. K.; Rabuck, A. D.; Raghavachari, K.; Foresman, J. B.; Ortiz, J. V.; Cui, Q.; Baboul, A. G.; Clifford, S.; Cioslowski, J.; Stefanov, B. B.; Liu, G.; Liashenko, A.; Piskorz, P.; Komaromi, I.; Martin, R. L.; Fox, D. J.; Keith, T.; Al-Laham, M. A.; Peng, C. Y.; Nanayakkara, A.; Challacombe, M.; Gill, P. M. W.; Johnson, B.; Chen, W.; Wong, M. W.; Gonzalez, C.; Pople, J. A. *Gaussian 03*; Gaussian, Inc.: Wallingford, CT, 2004.

(23) Beckman, J. S.; Chen, J.; Ischiropoulos, H.; Crow, J. P. Oxidative Chemistry of Peroxynitrite. In *Methods in Enzymology*; Packer, L., Ed.; Academic Press: San Diego, 1994; Vol. 233, pp 229−240.

(24) Whiteman, M.; Armstrong, J. S.; Cheung, N. S.; Siau, J.-L.; Rose, P.; Schantz, J.-T.; Jones, D. P.; Halliwell, B. *FASEB J.* **2004**, *18*, 1395.

(25) Whiteman, M.; Szabó, C.; Halliwell, B. *Br. J. Pharmacol.* **1999**, *126*, 1646.

(26) Olson, L. P.; Bartberger, M. D.; Houk, K. N. *J. Am. Chem. Soc.* **2003**, *125*, 3999.

(27) Luo, Y.-R. *Handbook of Bond Dissociation Energies in Organic Compounds*; CRC Press: Boca Raton, FL, 2003.

(28) Wang, L.; Roitberg, A.; Meuse, C.; Gaigalas, A. K. *Spectrochim. Acta, Part A* **2001**, *57*, 1781.

(29) Tamulis, A.; Tamuliene, J.; Balevicius, M. L.; Rinkevicius, Z.; Tamulis, V. *Struct. Chem.* **2003**, *14*, 643.

(30) Tremayne, M.; Kariuki, B. M.; Harris, K. D. M. *Angew. Chem., Int. Ed. Engl.* **1997**, *36*, 770.

(31) Ridley, J.; Zerner, M. C. *J. Mol. Spectrosc.* **1974**, *50*, 457.

(32) (a) Bauernschmitt, R.; Ahlrichs. *Chem. Phys. Lett.* **1996**, *256*, 454. (b) Casida, M. E.; Jamorski, C.; Casida, K. C.; Salahub, D. R. *J. Chem. Phys.* **1998**, *108*, 4439.

(33) Parker, C. A.; Rees, W. T. *Analyst* (*Cambridge, U.K.*) **1960**, *85*, 587.

(34) Dreuw, A.; Weisman, J. L.; Head-Gordon, M. *J. Chem. Phys.* **2003**, *119*, 2943.

(35) (a) Armstrong, D. A.; Waltz, W. L.; Rauk, A. *Can. J. Chem.* **2006**, *84*, 1614. (b) Bonini, M. G.; Augusto, O. *J. Biol. Chem.* **2001**, *276*, 9749. (c) Ferrer-Sueta, G.; Vitturi, D.; Batinic-Haberle, I.; Fridovich, I.; Goldstein, S. Gidon Czapski, G.; Radi, R. *J. Biol. Chem.* **2003**, *278*, 27432.

(36) (a) Czapski, G.; Lymar, S. V.; Schwarz, H. A. *J. Phys. Chem. A* **1999**, *103*, 3447. (b) Huie, R. E.; Clifton, C. L.; Neta, P. *Radiat. Phys. Chem.* **1991**, *38*, 477.

(37) Stanbury, D. M. *Adv. Inorg. Chem.* **1989**, *33*, 69.